

Supporting Information

Valley-selective carrier transfer in SnS-based van der Waals heterostructures

E. Sutter,^{1,*} H.-P. Komsa,² and P. Sutter^{3,*}

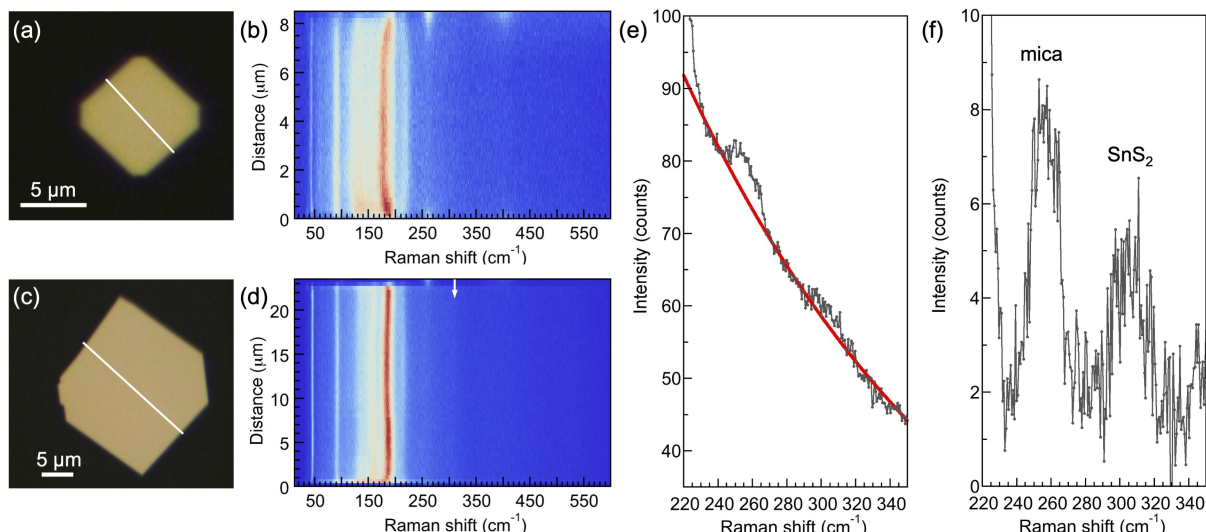
¹Department of Mechanical and Materials Engineering, University of Nebraska-Lincoln, Lincoln, NE 68588, USA

²Microelectronics Research Unit, University of Oulu, FI-90014, Oulu, Finland

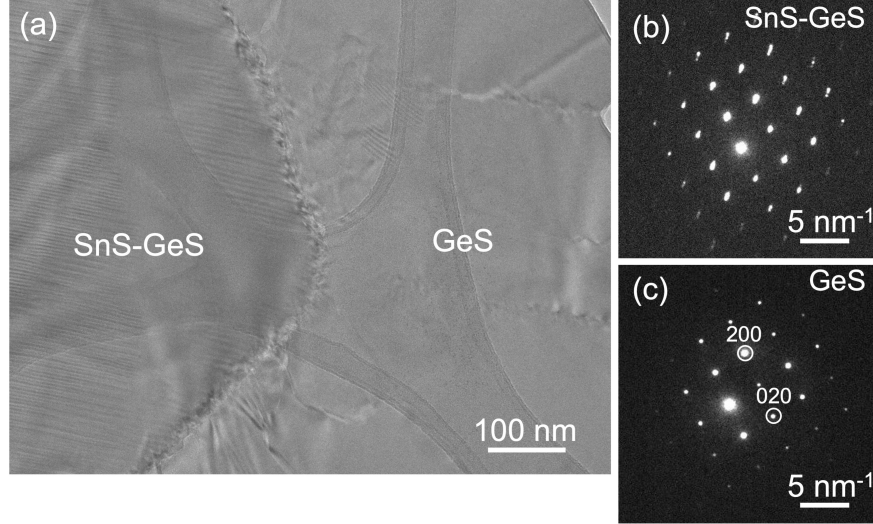
³Department of Electrical and Computer Engineering, University of Nebraska-Lincoln, Lincoln, NE 68588, USA

*Corresponding authors, email: esutter@unl.edu (E. Sutter), psutter@unl.edu (P. Sutter)

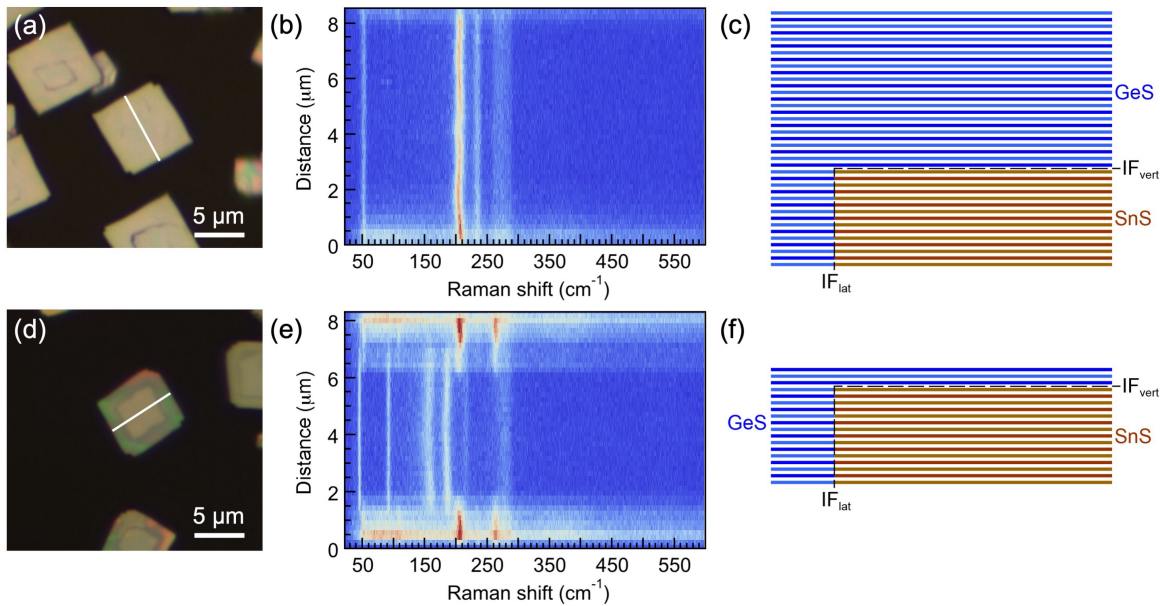
Supporting Figures



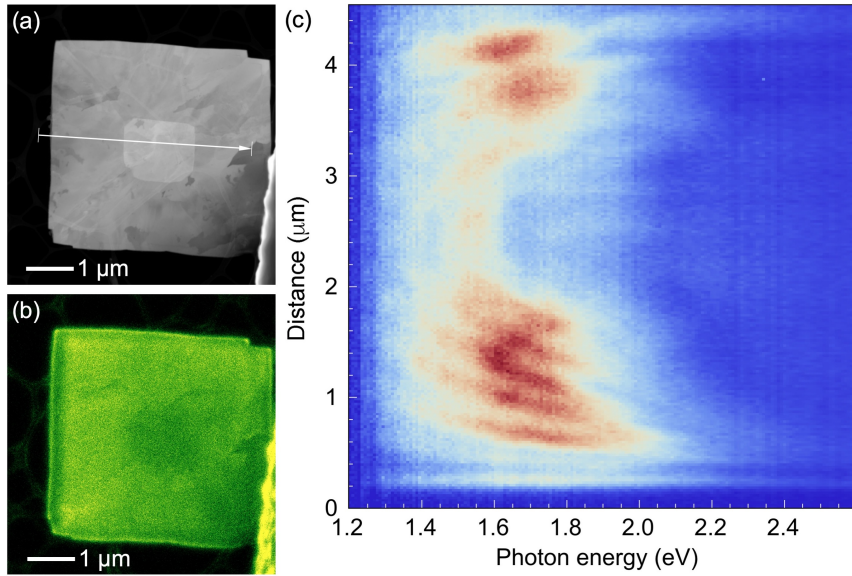
Supporting Figure 1. Raman spectroscopy of SnS flakes and SnS-SnS₂ heterostructures. (a) Optical microscopy of an SnS flake. (b) Raman linescan across the SnS flake (line in (a)), showing the characteristic Raman-active modes of SnS. (c) Optical microscopy of an SnS-SnS₂ wrap-around heterostructure, grown from SnS₂ precursor. (d) Raman linescan across the SnS-SnS₂ heterostructure (line in (c)). (e) Average of the individual Raman spectra along the linescan across the SnS-SnS₂ heterostructure (shown in (d)). (f) Average Raman spectrum across the SnS-SnS₂ heterostructure following background subtraction (red line in (e)). The mode at $\sim 256\text{ cm}^{-1}$ is due to residual signal from the mica substrate (also visible with higher intensity outside the SnS-SnS₂ flake), whereas the mode at $\sim 306\text{ cm}^{-1}$ originates from the thin SnS₂ shell covering the top of the flake.



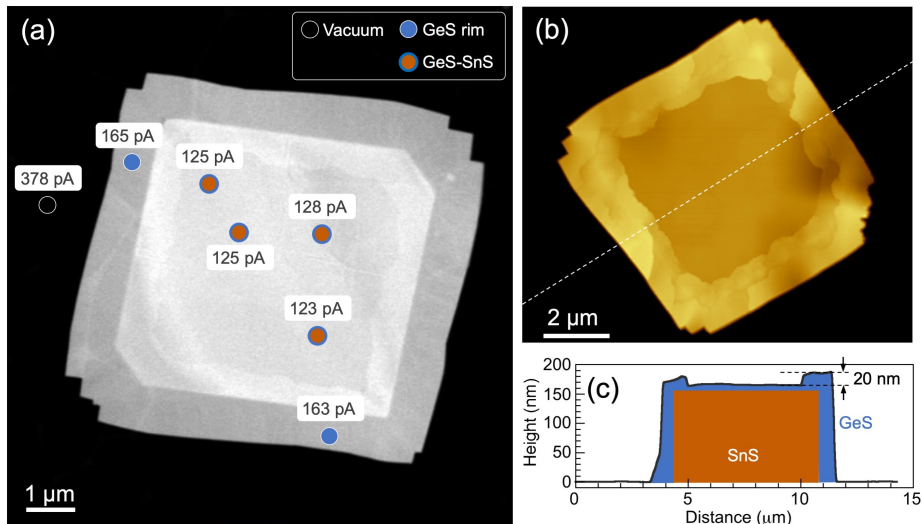
Supporting Figure 2. TEM imaging and nanobeam electron diffraction analysis of SnS-GeS heterostructures. (a) Plan-view TEM image obtained near the interface between the SnS seed covered by a thin (few-layer) GeS stack and the laterally attached GeS band (see Figure 2, main text). (b) Nanobeam electron diffraction pattern obtained within the SnS-GeS vertical stack, showing multiple reflections along the (100) axis, i.e., the direction with substantial ($\sim 10\%$) in-plane lattice mismatch between SnS and GeS while no extra spots appear along the (010) axis where the mismatch is negligible. (c) Nanobeam electron diffraction within the laterally attached GeS edge band, showing a single-phase GeS diffraction pattern.



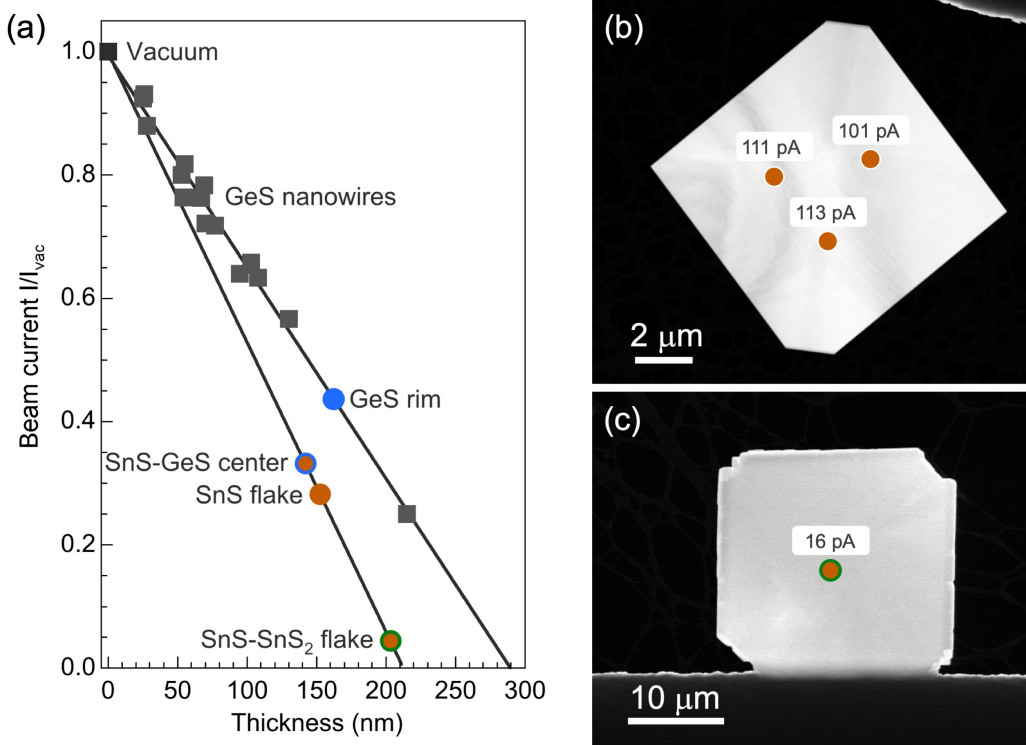
Supporting Figure 3. Raman spectroscopy of SnS-GeS heterostructures. (a) Optical microscopy of an SnS-GeS heterostructure with thick GeS coverage. (b) Raman linescan across the SnS flake (line in (a)), showing the characteristic Raman-active modes of SnS. (c) Schematic of the SnS-GeS heterostructure with thick GeS vertical layer stack. (d) Optical microscopy of an SnS-SnS₂ wrap-around heterostructure, grown from SnS₂ precursor. (e) Raman linescan across the SnS-SnS₂ heterostructure (line in (d)). (f) Schematic of the SnS-GeS heterostructure with thin GeS vertical stack.



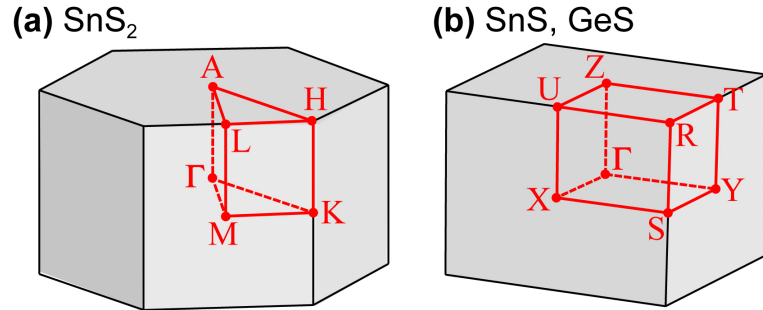
Supporting Figure 4. Cathodoluminescence of SnS-GeS lateral heterostructures with small SnS seed crystals and narrow GeS rims. **(a)** HAADF-STEM image of a SnS-GeS heterostructure. **(b)** Panchromatic STEM-CL map of the heterostructure shown in (a). **(c)** Hyperspectral STEM-CL linescan along the line shown in (a), illustrating the fringe pattern due to interference of edge-reflected waveguide modes reaching up to $\sim 2 \mu\text{m}$ into the interior of the flakes.



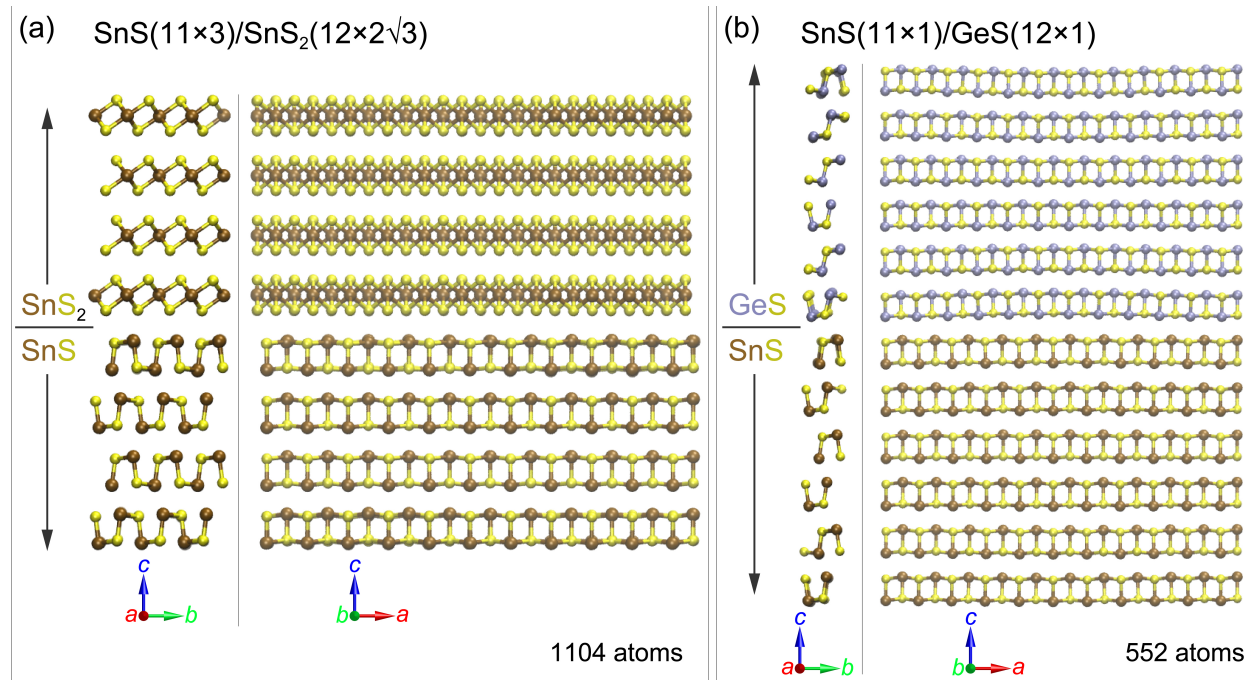
Supporting Figure 5. Thickness calibration on SnS-GeS heterostructures based on beam-current attenuation measurements on GeS nanowires (see also Supporting Figure 3). **(a)** HAADF-STEM image of a SnS-GeS heterostructure with local beam-current measurements. The current of the unattenuated electron beam in vacuum is 378 pA, while transit through GeS and SnS causes an attenuation of the measured beam current that scales with the thickness of the flakes. The thickness of the vertical SnS-GeS heterostructure near the center is estimated based on beam-current attenuation measurements in the pure GeS rim and taking into account the morphology of the heterostructures determined by atomic force microscopy (AFM). **(b)** Tapping mode AFM image of a representative SnS-GeS heterostructure. **(c)** Thickness profile extracted along the dashed line in (b). Note the $\sim 20 \text{ nm}$ elevated thickness due to combined lateral and vertical GeS growth near the edge, leading up to a GeS overlayer thickness that is reduced to a few nm in the central region.



Supporting Figure 6. Thickness calibration on SnS-GeS heterostructures based on beam-current attenuation measurements on GeS nanowires. **(a)** Plot of beam-current attenuation measurements on GeS nanowires with different diameters (gray squares) along with beam-current measurements on SnS-GeS heterostructures, pure SnS flakes, and SnS-SnS₂ wrap-around core-shell heterostructures (round symbols). The calibration on nanowires with different diameters allows the measured electron beam current on the pure GeS rim of SnS-GeS heterostructures (see Supporting Figure 2) to be translated into thickness of the rim (162 nm, blue dot). From AFM imaging (see, e.g., Supporting Figure 2 (c)) we find that the rim is typically ~20 nm thicker than the vertical SnS-GeS stack near in the central region. This yields the center thickness of the vertical SnS-GeS heterostructure (142 nm, brown/blue dot) analyzed by STEM-CL (Figure 5 (d)-(f), main text). Since the SnS-GeS vertical stack consists primarily (~95%) of SnS, this also yields a good estimate for the beam-current attenuation of homogeneous SnS flakes and SnS-SnS₂ core-shell heterostructures. Using this calibration, we find that the samples analyzed by STEM-CL have thickness of 152 nm (homogeneous SnS flake, brown dot; see Figure 4, main text) and 203 nm (SnS-SnS₂ core-shell heterostructure, brown/green dot; see Figure 5 (a)-(c), main text), respectively. **(b)** HAADF-STEM image of a homogeneous SnS flake analyzed by STEM-CL with representative beam-current attenuation measurements. **(c)** HAADF-STEM image of an SnS-SnS₂ core-shell heterostructure analyzed by STEM-CL with beam-current attenuation measurement near the center.



Supporting Figure 7. Brillouin zones of (a) SnS_2 and (b) SnS , GeS . High-symmetry points are marked with the same labeling as in the calculated band structures shown in the main text.



Supporting Figure 8. Interface models used to determine the band offsets between (a) (SnS , SnS_2) and (b) (SnS , GeS) in van der Waals heterostructures. Both panels (a) and (b) show side views of the computational cells, seen along the in-plane a -axis (left) and b -axis (right), respectively.

Raw data of plots:

1. Figure 4(d)

Photon energy (eV)	Relative intensity
1.1427	0.061798
1.1499	0.2558
1.1572	0.091687
1.1644	0.15731
1.1716	0.071648
1.1789	0.10194
1.1861	0.12968
1.1933	0.32188
1.2006	0.21398
1.2078	0.25196
1.215	0.26045
1.2223	0.38738
1.2295	0.33159
1.2368	0.4284
1.244	0.52205
1.2512	0.53778
1.2585	0.5108
1.2657	0.50749
1.2729	0.6152
1.2802	0.52292
1.2874	0.46423
1.2946	0.61538
1.3019	0.55463
1.3091	0.58588
1.3164	0.67151
1.3236	0.65861
1.3308	0.70181
1.3381	0.73115
1.3453	0.7716
1.3525	0.72656
1.3598	0.73779
1.367	0.82009
1.3742	0.71703
1.3815	0.74117
1.3887	0.73781
1.396	0.7789
1.4032	0.77473

1.4104	0.72586
1.4177	0.65636
1.4249	0.58238
1.4321	0.65747
1.4394	0.66753
1.4466	0.64833
1.4539	0.5737
1.4611	0.56696
1.4683	0.61946
1.4756	0.53903
1.4828	0.40362
1.49	0.38619
1.4973	0.39993
1.5045	0.33244
1.5117	0.41504
1.519	0.40955
1.5262	0.35831
1.5335	0.34484
1.5407	0.36569
1.5479	0.36819
1.5552	0.3711
1.5624	0.43221
1.5696	0.45229
1.5769	0.47334
1.5841	0.46503
1.5913	0.51372
1.5986	0.53344
1.6058	0.57307
1.6131	0.58945
1.6203	0.65567
1.6275	0.64733
1.6348	0.63163
1.642	0.62911
1.6492	0.656
1.6565	0.69032
1.6637	0.68919
1.6709	0.74474
1.6782	0.73301
1.6854	0.78066
1.6927	0.77646

1.6999	0.78624
1.7071	0.85042
1.7144	0.89429
1.7216	0.90607
1.7288	0.89999
1.7361	0.84858
1.7433	0.92819
1.7505	0.92515
1.7578	0.93682
1.765	0.92654
1.7723	0.94289
1.7795	0.98472
1.7867	1
1.794	0.92205
1.8012	0.88938
1.8084	0.92088
1.8157	0.9255
1.8229	0.8923
1.8302	0.85471
1.8374	0.9195
1.8446	0.90571
1.8519	0.90225
1.8591	0.90027
1.8663	0.87792
1.8736	0.85719
1.8808	0.83713
1.888	0.82732
1.8953	0.83256
1.9025	0.85376
1.9098	0.86672
1.917	0.86562
1.9242	0.84661
1.9315	0.81899
1.9387	0.80294
1.9459	0.79151
1.9532	0.77134
1.9604	0.74304
1.9676	0.7784
1.9749	0.78718
1.9821	0.73822

1.9894	0.74451
1.9966	0.73663
2.0038	0.73011
2.0111	0.73886
2.0183	0.75961
2.0255	0.75489
2.0328	0.7425
2.04	0.72163
2.0472	0.71349
2.0545	0.70117
2.0617	0.67774
2.069	0.65378
2.0762	0.63627
2.0834	0.65223
2.0907	0.65415
2.0979	0.6447
2.1051	0.64988
2.1124	0.64387
2.1196	0.60342
2.1269	0.61655
2.1341	0.66522
2.1413	0.62637
2.1486	0.58632
2.1558	0.57568
2.163	0.5838
2.1703	0.61252
2.1775	0.5972
2.1847	0.56555
2.192	0.56142
2.1992	0.55586
2.2065	0.53646

2. Figure 7(c)

Photon energy (eV)	Relative intensity
1.1427	-0.047341
1.1499	0.033223
1.1572	0.073834
1.1644	0.086
1.1716	-0.029042
1.1789	0.014671
1.1861	0.11108

1.1933	0.1644
1.2006	0.23897
1.2078	0.21126
1.215	0.29738
1.2223	0.2061
1.2295	0.27461
1.2368	0.3583
1.244	0.36944
1.2512	0.46401
1.2585	0.60892
1.2657	0.47408
1.2729	0.52955
1.2802	0.65511
1.2874	0.68935
1.2946	0.7348
1.3019	0.67492
1.3091	0.70517
1.3164	0.70059
1.3236	0.75827
1.3308	0.74192
1.3381	0.78119
1.3453	0.813
1.3525	0.82054
1.3598	0.76725
1.367	0.9139
1.3742	0.87953
1.3815	0.92529
1.3887	1
1.396	0.99338
1.4032	0.90335
1.4104	0.9419
1.4177	0.8659
1.4249	0.87837
1.4321	0.78262
1.4394	0.84432
1.4466	0.76421
1.4539	0.75536
1.4611	0.70085
1.4683	0.66376
1.4756	0.65928

1.4828	0.53333
1.49	0.58668
1.4973	0.57047
1.5045	0.60379
1.5117	0.6014
1.519	0.62675
1.5262	0.63881
1.5335	0.75512
1.5407	0.69031
1.5479	0.73269
1.5552	0.76088
1.5624	0.72652
1.5696	0.72362
1.5769	0.74088
1.5841	0.78041
1.5913	0.81804
1.5986	0.80307
1.6058	0.8054
1.6131	0.78357
1.6203	0.75931
1.6275	0.78999
1.6348	0.78218
1.642	0.89213
1.6492	0.85758
1.6565	0.83051
1.6637	0.86113
1.6709	0.8511
1.6782	0.84936
1.6854	0.87631
1.6927	0.86336
1.6999	0.89852
1.7071	0.87931
1.7144	0.86436
1.7216	0.91667
1.7288	0.95504
1.7361	0.93114
1.7433	0.91398
1.7505	0.92353
1.7578	0.93473
1.765	0.94071

1.7723	0.90277
1.7795	0.8633
1.7867	0.85885
1.794	0.86171
1.8012	0.86721
1.8084	0.94311
1.8157	0.87379
1.8229	0.88714
1.8302	0.90643
1.8374	0.79093
1.8446	0.79959
1.8519	0.82985
1.8591	0.84
1.8663	0.80544
1.8736	0.78427
1.8808	0.79167
1.888	0.76542
1.8953	0.78935
1.9025	0.8328
1.9098	0.80244
1.917	0.77637
1.9242	0.75339
1.9315	0.7465
1.9387	0.68275
1.9459	0.62299
1.9532	0.70196
1.9604	0.74084
1.9676	0.74985
1.9749	0.72523
1.9821	0.72211
1.9894	0.71397
1.9966	0.69757
2.0038	0.6877
2.0111	0.6872
2.0183	0.69642
2.0255	0.696
2.0328	0.69087
2.04	0.68027
2.0472	0.682
2.0545	0.68327

2.0617	0.6809
2.069	0.64449
2.0762	0.61121
2.0834	0.6486
2.0907	0.65206
2.0979	0.62801
2.1051	0.61336
2.1124	0.60943
2.1196	0.6323
2.1269	0.68016
2.1341	0.74432
2.1413	0.63935
2.1486	0.55008
2.1558	0.58815
2.163	0.61029
2.1703	0.61502
2.1775	0.58437
2.1847	0.54084
2.192	0.54309
2.1992	0.54846
2.2065	0.55879

3. Figure 7(f)

Photon energy (eV)	Relative intensity
1.1973	0.26205
1.2057	0.43349
1.2141	0.51351
1.2225	0.76092
1.2309	0.86877
1.2393	1.036
1.2477	1.3507
1.2561	1.5563
1.2645	1.8023
1.2729	2.0187
1.2813	2.0727
1.2896	2.2519
1.298	2.338
1.3064	2.351
1.3148	2.265
1.3232	2.1533
1.3316	2.1664

1.34	2.1371
1.3484	2.0095
1.3568	1.9685
1.3652	2.0529
1.3736	2.0568
1.382	1.9586
1.3903	2.0086
1.3987	2.0717
1.4071	2.06
1.4155	2.0357
1.4239	2.041
1.4323	1.9867
1.4407	2.0827
1.4491	1.9572
1.4575	1.9591
1.4659	1.9138
1.4743	1.8717
1.4827	1.8608
1.4911	1.7416
1.4995	1.7229
1.5078	1.6602
1.5162	1.649
1.5246	1.5974
1.533	1.531
1.5414	1.5149
1.5498	1.511
1.5582	1.5798
1.5666	1.4387
1.575	1.5158
1.5834	1.4526
1.5918	1.4815
1.6002	1.5229
1.6086	1.5031
1.6169	1.473
1.6253	1.509
1.6337	1.5578
1.6421	1.4557
1.6505	1.5011
1.6589	1.5473
1.6673	1.5779

1.6757	1.5472
1.6841	1.5212
1.6925	1.5129
1.7009	1.4825
1.7093	1.4582
1.7177	1.4951
1.726	1.4525
1.7344	1.429
1.7428	1.4411
1.7512	1.3926
1.7596	1.3836
1.768	1.3132
1.7764	1.3468
1.7848	1.3318
1.7932	1.2695
1.8016	1.3458
1.81	1.2573
1.8184	1.2569
1.8268	1.2561
1.8351	1.2774
1.8435	1.2666
1.8519	1.2526
1.8603	1.2254
1.8687	1.2157
1.8771	1.2223
1.8855	1.1496
1.8939	1.235
1.9023	1.1907
1.9107	1.1831
1.9191	1.1751
1.9275	1.1794
1.9359	1.2055
1.9442	1.2335
1.9526	1.2367
1.961	1.2165
1.9694	1.2122
1.9778	1.2247
1.9862	1.2395
1.9946	1.2344
2.003	1.2291

2.0114	1.228
2.0198	1.2369
2.0282	1.2702
2.0366	1.2612
2.045	1.2542
2.0533	1.2532
2.0617	1.2482
2.0701	1.2479
2.0785	1.2503
2.0869	1.2553
2.0953	1.2721
2.1037	1.2614
2.1121	1.2382
2.1205	1.2247
2.1289	1.2328
2.1373	1.2429
2.1457	1.2439
2.1541	1.2357
2.1624	1.225
2.1708	1.2127
2.1792	1.2193
2.1876	1.2309
2.196	1.2456
2.2044	1.243

4. Supporting Figure 1(e)

Raman shift (cm ⁻¹)	Intensity (arb. units)
220.2	115.54
220.88	110.07
221.56	109.88
222.25	104.9
222.93	102.37
223.61	99.585
224.3	99.39
224.98	98.659
225.66	95.195
226.35	92.415
227.03	91.732
227.71	90.415
228.39	90.561
229.07	89.39

229.76	87.585
230.44	87.878
231.12	87.439
231.8	85.244
232.49	85.341
233.17	83.537
233.85	83.683
234.53	84.415
235.21	83.439
235.89	83.683
236.57	83.732
237.26	82.366
237.94	82.561
238.62	81.634
239.3	83.732
239.98	81.39
240.66	81.195
241.34	81.781
242.02	81.244
242.7	81.39
243.38	81.049
244.06	80.415
244.74	81.927
245.42	81.488
246.1	79.976
246.78	82.073
247.46	79.683
248.14	81.341
248.82	81.878
249.5	82.854
250.18	82.805
250.85	80.659
251.53	80.707
252.21	81.049
252.89	82.463
253.57	81.049
254.25	80.854
254.93	81.049
255.6	79.976
256.28	80.463

256.96	79.927
257.64	80.317
258.32	78.073
258.99	79.244
259.67	77.878
260.35	77.537
261.03	77.341
261.7	75.976
262.38	77.439
263.06	76.902
263.74	74.951
264.41	76.561
265.09	75.439
265.77	72.805
266.44	72.61
267.12	71.976
267.8	69.878
268.47	70.561
269.15	70.415
269.82	70.171
270.5	69.439
271.17	68.902
271.85	68.561
272.53	67.195
273.2	67.683
273.88	67.537
274.55	68.805
275.23	68.171
275.9	67.585
276.58	65.927
277.25	65.927
277.93	65.049
278.6	65.976
279.28	64.854
279.95	66.317
280.63	65.878
281.3	64.073
281.98	64.415
282.65	63.537
283.32	63.488

284	64.122
284.67	63.878
285.35	63.146
286.02	63.732
286.69	62.707
287.36	63.195
288.04	62.22
288.71	60.951
289.39	62.951
290.06	62.024
290.73	59.732
291.4	60.61
292.08	60.171
292.75	62.707
293.42	61.293
294.09	59.537
294.77	62.317
295.44	59.976
296.11	62.268
296.78	61.488
297.45	62.366
298.13	60.512
298.8	61.488
299.47	59.927
300.14	58.659
300.81	61.049
301.48	59.244
302.15	60.561
302.82	58.561
303.5	60.171
304.17	60.171
304.84	59
305.51	59.927
306.18	58.122
306.85	57.976
307.52	57.244
308.19	58.024
308.86	58.512
309.53	57.146
310.2	57.195

310.87	59.146
311.54	55.537
312.21	56.024
312.88	55.195
313.55	55.293
314.21	53.976
314.88	53.244
315.55	55.439
316.22	53.829
316.89	53.829
317.56	55.146
318.23	54.805
318.9	51.683
319.57	53.78
320.23	52.366
320.9	51.732
321.57	50.317
322.24	50.61
322.91	50.463
323.57	49.927
324.24	50.415
324.91	49.683
325.58	50.171
326.24	51.098
326.91	49.829
327.58	48.805
328.25	50.171
328.91	50.024
329.58	46.073
330.25	46.561
330.91	49.537
331.58	48.171
332.25	46.805
332.91	47.293
333.58	47.878
334.24	47.195
334.91	48.61
335.58	46.659
336.24	46.659
336.91	46.561

337.57	46.024
338.24	45.195
338.9	46.22
339.57	46.512
340.24	45.244
340.9	46.171
341.57	46.024
342.23	45.78
342.89	46.024
343.56	45.878
344.23	46.61
344.89	45.634
345.55	46.268
346.22	45.293
346.88	44.171
347.55	44.707
348.21	44.805
348.87	43.732
349.54	44.463
350.2	45.39
350.86	45.829

5. Supporting Figure1 (f)

Raman shift (cm ⁻¹)	Intensity (arb. units)
220.2	26.31
220.88	21.199
221.56	21.353
222.25	16.727
222.93	14.538
223.61	12.103
224.3	12.253
224.98	11.865
225.66	8.7441
226.35	6.304
227.03	5.9602
227.71	4.9819
228.39	5.4648
229.07	4.6292
229.76	3.1584
230.44	3.7847
231.12	3.6765

231.8	1.8115
232.49	2.2375
233.17	0.7602
233.85	1.2324
234.53	2.2892
235.21	1.637
235.89	2.203
236.57	2.5732
237.26	1.5271
237.94	2.0406
238.62	1.431
239.3	3.8446
239.98	1.8179
240.66	1.9356
241.34	2.8334
242.02	2.608
242.7	3.0639
243.38	3.0305
244.06	2.7039
244.74	4.5222
245.42	4.3877
246.1	3.1792
246.78	5.5789
247.46	3.49
248.14	5.4494
248.82	6.2842
249.5	7.5578
250.18	7.805
250.85	5.9534
251.53	6.2968
252.21	6.9309
252.89	8.6383
253.57	7.5137
254.25	7.6078
254.93	8.0911
255.6	7.3058
256.28	8.0796
256.96	7.8275
257.64	8.5016
258.32	6.54

258.99	7.9924
259.67	6.9076
260.35	6.8456
261.03	6.9286
261.7	5.8397
262.38	7.5794
263.06	7.3177
263.74	5.6403
264.41	7.5221
265.09	6.6719
265.77	4.3085
266.44	4.3831
267.12	4.0176
267.8	2.1878
268.47	3.1366
269.15	3.2554
269.82	3.2761
270.5	2.8073
271.17	2.5329
271.85	2.4532
272.53	1.3467
273.2	2.0942
273.88	2.2054
274.55	3.731
275.23	3.3528
275.9	3.0228
276.58	1.6179
277.25	1.8713
277.93	1.245
278.6	2.4233
279.28	1.5513
279.95	3.2635
280.63	3.0725
281.3	1.5153
281.98	2.1024
282.65	1.4695
283.32	1.6649
284	2.5426
284.67	2.5411
285.35	2.0505

286.02	2.8764
286.69	2.0913
287.36	2.8174
288.04	2.0796
288.71	1.0479
289.39	3.2836
290.06	2.5915
290.73	0.53273
291.4	1.6438
292.08	1.4362
292.75	4.204
293.42	3.0198
294.09	1.4932
294.77	4.5017
295.44	2.388
296.11	4.9073
296.78	4.3522
297.45	5.4551
298.13	3.8258
298.8	5.0239
299.47	3.6856
300.14	2.6382
300.81	5.2491
301.48	3.6637
302.15	5.1999
302.82	3.4174
303.5	5.2445
304.17	5.4604
304.84	4.5048
305.51	5.6465
306.18	4.0552
306.85	4.1215
307.52	3.6016
308.19	4.5938
308.86	5.2916
309.53	4.1352
310.2	4.3924
310.87	6.5515
311.54	3.1486
312.21	3.8428

312.88	3.2188
313.55	3.5212
314.21	2.4079
314.88	1.8791
315.55	4.2764
316.22	2.8685
316.89	3.0692
317.56	4.5861
318.23	4.4439
318.9	1.5198
319.57	3.8148
320.23	2.5972
320.9	2.1592
321.57	0.93949
322.24	1.4269
322.91	1.4743
323.57	1.1304
324.24	1.8105
324.91	1.2701
325.58	1.9487
326.24	3.0655
326.91	1.9866
327.58	1.1503
328.25	2.7041
328.91	2.7449
329.58	-1.0203
330.25	-0.3466
330.91	2.8136
331.58	1.6317
332.25	0.44974
332.91	1.1201
333.58	1.8873
334.24	1.3854
334.91	2.9806
335.58	1.2092
336.24	1.3887
336.91	1.4697
337.57	1.1107
338.24	0.4586
338.9	1.6593

339.57	2.1279
340.24	1.0345
340.9	2.1351
341.57	2.1627
342.23	2.0918
342.89	2.5081
343.56	2.5334
344.23	3.4363
344.89	2.6305
345.55	3.4345
346.22	2.6281
346.88	1.6741
347.55	2.3784
348.21	2.6433
348.87	1.7362
349.54	2.6337
350.2	3.7255
350.86	4.3294

6. Supporting Figure6 (a)

Sample	Known thickness (nm)	Relative beam current
Vacuum	0	1.00
GeS nanowire	55	0.82
GeS nanowire	28	0.88
GeS nanowire	69	0.78
GeS nanowire	26	0.93
GeS nanowire	54	0.76
GeS nanowire	77	0.72
GeS nanowire	25	0.92
GeS nanowire	70	0.72
GeS nanowire	108	0.63
GeS nanowire	130	0.57
GeS nanowire	95	0.64
GeS nanowire	53	0.80
GeS nanowire	103	0.66

Sample	Inferred thickness (nm)	Relative beam current
GeS rim	162.3	0.44
SnS-GeS center	142.3	0.33
SnS flake	152.7	0.28
SnS-SnS ₂ flake	203.5	0.04

